

# Polarization-Sensitive Structural Colors with Hue-and-Saturation Tuning Based on All-Dielectric Nanopixels

Bo Yang, Wenwei Liu, Zhancheng Li, Hua Cheng, Shuqi Chen,\* and Jianguo Tian

**Structural colors generated by the plasmonic resonance of metallic nanostructures, particularly aluminum, have been intensively studied in recent years. However, the inherent Ohmic loss and interband transitions in metals hinder the high efficiency and narrow bandwidth required for pure colors. Here, arrays of asymmetric titanium oxide elliptical nanopixels on a silica substrate are utilized to realize polarization-sensitive structural colors with high saturation, high efficiency (more than 90%), and high resolution. Owing to Fano resonance resulting from the interference between the radiating waves of dipole resonances and directly reflected waves, perfect narrow reflected spectra can be formed with nearly ideal efficiency in the visible spectrum based on this all-dielectric nanostructure. In particular, hue- and saturation-tuned colors can be simultaneously obtained under two orthogonally polarized incident lights with apparent color contrast. Based on the superior properties of the titanium oxide metasurface, the proposed design strategy is anticipated to form a new paradigm for practical applications, such as high-density optical data storage, nanoscale optical elements, sensing, security, and so on.**

For several years, organic dyes and chemical pigments formed the most common materials for imaging and display technologies.<sup>[1–4]</sup> However, the resolution of these pigments is not sufficient, and they cannot endure durative high-intensity or high-temperature illumination.<sup>[1–6]</sup> In addition, these pigments are environment-unfriendly and expensive from the perspective of recycling.<sup>[4]</sup> In this context, recently, structural colors have attracted considerable attention as an alternative to pigments since they offer high resolution, are eco-friendly, and can be tuned dynamically.<sup>[1–3,7–10]</sup> Structural colors generated from plasmonic metasurfaces via surface plasmon resonance have been extensively investigated.<sup>[11–13]</sup> The building blocks of plasmonic metasurfaces include gold,<sup>[14]</sup> silver,<sup>[5,8,15]</sup> and


aluminum.<sup>[1–4,7,9,16–18]</sup> In the early stages, gold and silver were the preferred choices to achieve structural colors. However, gold is expensive and undergoes interband transitions at wavelengths in the range from 400 to 500 nm, while silver is easily oxidized and sulfated in ambient air.<sup>[1–4]</sup> On the contrary, aluminum is a promising substitute that is not only stable but also inexpensive. In recent years, several investigations on structural colors generated by aluminum nanostructures have been realized. Yang et al. have utilized aluminum metasurfaces to realize color palettes for photorealistic printing.<sup>[2]</sup> Nevertheless, because of the inherent Ohmic loss in metals, the plasmon resonance peak is relatively small (and thus inefficient) and typically spreads over a broad spectral band, thereby leading to low color saturation and purity.<sup>[7]</sup>

In order to overcome these limitations, an alternative material with negligible absorption and relatively high refractive index is highly desired to realize pure and highly saturated structural colors. Recent investigations on dielectric materials have demonstrated that all-dielectric metasurfaces (particularly silicon) exhibit remarkable performances with low loss and strong dipole resonances in the infrared spectral range. All-dielectric silicon metasurfaces have been extensively applied to act as Huygens' surfaces, multi-wavelength achromatic metasurfaces, dielectric gradient metasurfaces, and so on.<sup>[19–23]</sup> Nonetheless, amorphous silicon exhibits high absorption of wavelengths from 400 to 500 nm, which means that it is difficult to realize high efficiency and narrow bandwidth for color generation, especially for blue colors.<sup>[24–27]</sup> Hence, amorphous titanium oxide, with its negligible loss and relatively high refractive index in the visible spectral range, is considered as a suitable choice to address these challenges.<sup>[28,29]</sup> Thus far, titanium oxide metasurfaces have been utilized in many applications, such as high-numerical-aperture metalenses in the visible range, color holograms, and wearable optics.<sup>[30,31]</sup>

In this study, we present the strategy of polarization-dependent color generation with subwavelength resolution in the reflection mode across the visible range by utilizing amorphous titanium oxide elliptical nanopixels deposited on a silica substrate. We demonstrate that titanium oxide is a remarkable material to generate structural colors owing to the phenomenon of Fano resonance and the presence of the photonic band gap. In addition, we realize the sharp contrast of colors under two orthogonally polarization states of incident light by varying the

Dr. B. Yang, Dr. W. Liu, Dr. Z. Li, Prof. H. Cheng, Prof. S. Chen, Prof. J. Tian  
The Key Laboratory of Weak Light Nonlinear Photonics  
Ministry of Education  
School of Physics and TEDA Institute of Applied Physics  
Nankai University  
Tianjin 300071, China  
E-mail: schen@nankai.edu.cn

Prof. H. Cheng, Prof. S. Chen, Prof. J. Tian  
The Collaborative Innovation Center of Extreme Optics  
Shanxi University  
Taiyuan, Shanxi 030006, China

 The ORCID identification number(s) for the author(s) of this article can be found under <https://doi.org/10.1002/adom.201701009>.

DOI: 10.1002/adom.201701009

periods of the nanopixels along the  $x$ - and  $y$ -axes. In particular, we simultaneously realize the hue-and-saturation tuning in  $x$ - and  $y$ -polarization states by varying the period in one direction. We also obtain three-primary-color switching (green to blue, blue to red, and red to green) by varying the polarization degree from  $0^\circ$  to  $90^\circ$ , which can be extensively employed in information coding and display technologies.

The proposed pixels are composed of asymmetric elliptic titanium oxide nanopillars on a rectangular silica substrate with varying diameters and periods along the  $x$ - and  $y$ -directions, which are referred to as  $P_x$  and  $P_y$ , respectively, as illustrated in Figure 1a. The height ( $H$ ) of the nanopillars is fixed at 300 nm. The major and minor axes of the ellipse are notated as  $a$  and  $b$ , respectively. The angle between the polarization of the incident light and  $x$ -axis is defined as  $\phi$ . The incident  $x$ -polarized white light can be filtered into various visible colors by varying the geometric parameters of the nanopixels, as shown in Figure 1a. Meanwhile, the asymmetric nanopixels can generate distinct colors for the same nanostructure under two orthogonal polarizations, as shown in Figure 1a,b. The light–matter interaction is simulated by finite-element method (commercial

software COMSOL Multiphysics) with periodic boundary conditions in the  $x$ - and  $y$ -directions to model infinite arrays and perfect match layer in the  $z$ -direction to mimic a free space.<sup>[32]</sup> The refractive index of amorphous titanium oxide gradually varies with wavelength, and the absorption coefficient can be negligible in the visible range.<sup>[25,31]</sup> The refractive index of silica is set as 1.45.<sup>[25]</sup>

In order to cover the full color palette, we change the periods of the nanopixel along the  $x$ - and  $y$ -directions in the range of 300 to 400 nm with a 25 nm interval. Figure 1c,d schematically shows the virtual colors of the nanopillars array by varying  $P_x$  and  $P_y$  under  $x$ - and  $y$ -polarized incident lights, respectively. The duty ratio is fixed at 0.6 (the corresponding diameters are 180, 195, 210, 225, and 240 nm in that order along both directions), which is defined as the ratio of the major axes and minor axes  $a/b$  of the pixels to the period  $P_x/P_y$ . A sharp color contrast can be obtained under two orthogonally polarized incident lights for each nanostructure set. Figure 1c shows the colors can change from blue to green to red with increasing  $P_x$  for  $x$ -polarized incidence, where  $P_y$  is fixed at 300 nm. All the pixels exhibit distinct saturation of blue for  $y$ -polarized incidence. The

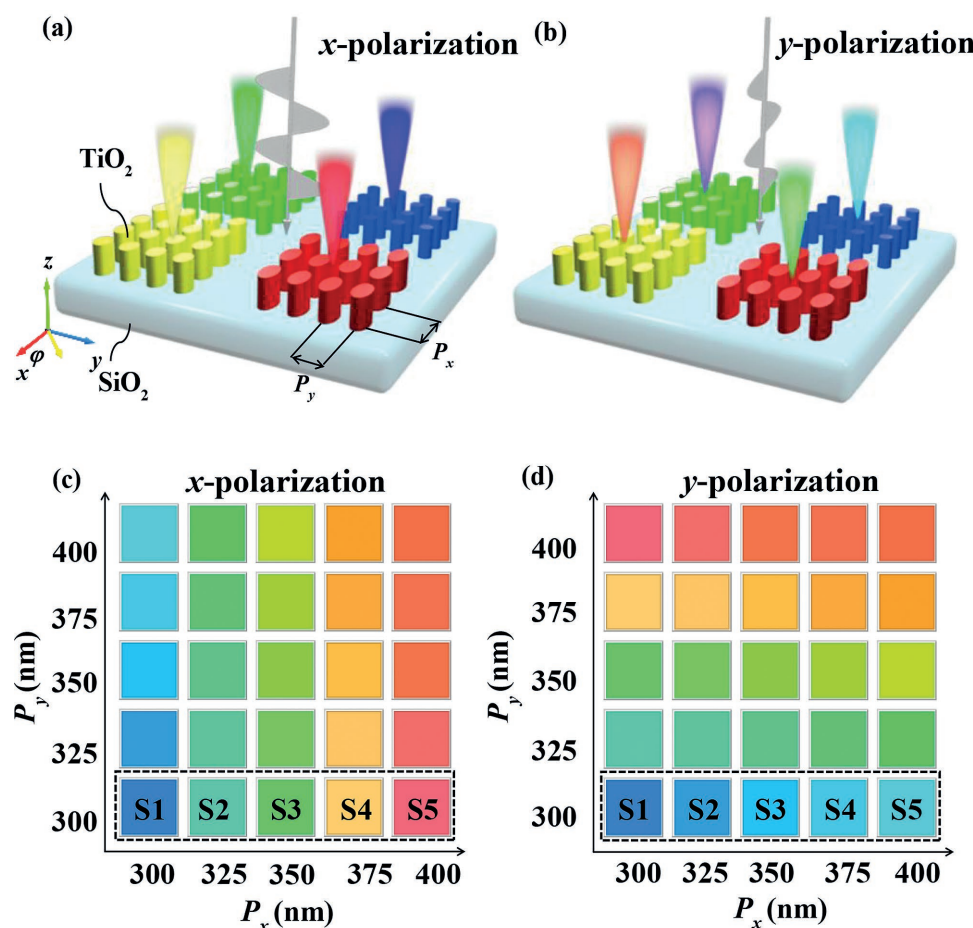


**Figure 1.** Top: Schematic illustrating the architecture of all-dielectric color filter with periodic titanium oxide elliptical nanopixels on silica substrate. With the same structure, a)  $x$ -polarized and b)  $y$ -polarized incident white light is scattered back into distinct visible colors due to the asymmetry of nanopixels. The lattice dimensions of the device are  $P_x$  and  $P_y$  along the  $x$ - and  $y$ -directions, respectively. Bottom: The color palettes for connected arrays of elliptical pixels with varying periods  $P_x$  and  $P_y$ , with step size of 25 nm. The color palettes show reflected color illuminated under c)  $x$ -polarized and d)  $y$ -polarized light. The color is obtained via computing the reflection spectrum onto an RGB set.

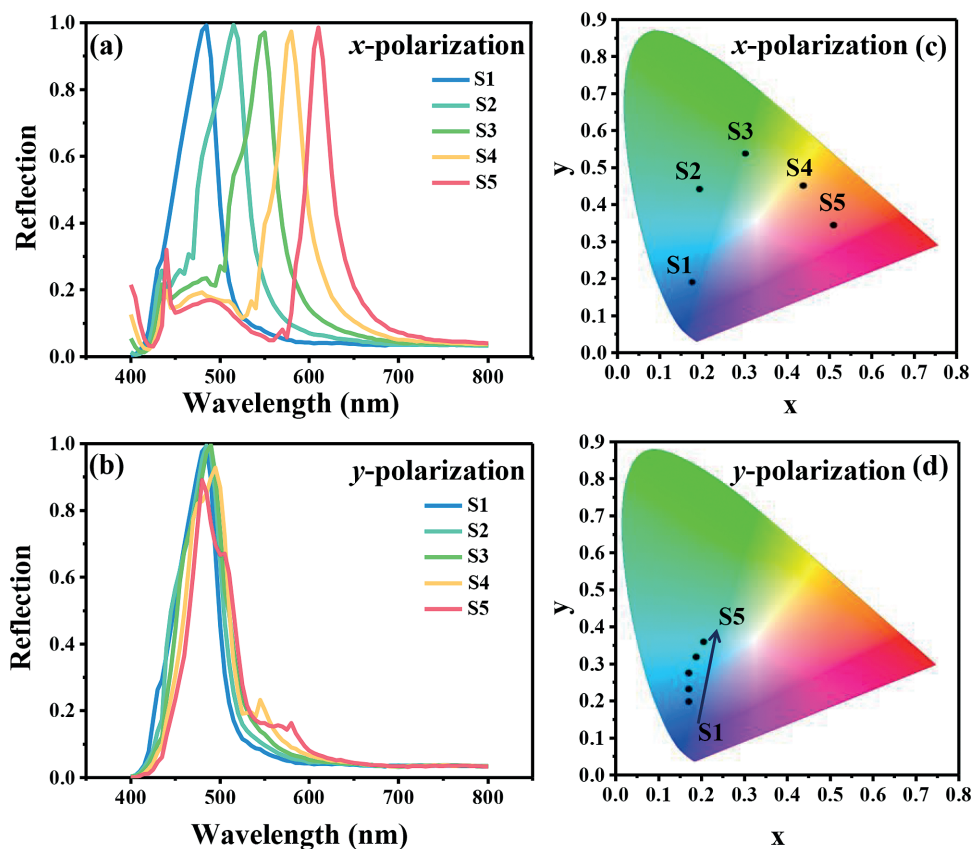


**Figure 2.** Polarization-tuned reflection spectra of pixels indicated by dashed boxes in Figure 1 along with corresponding incident angle dependence. Simulated reflection spectra obtained upon increasing  $P_x$  from 300 to 400 nm in a step of 25 nm under a)  $x$ -polarized and b)  $y$ -polarized light. The corresponding CIE 1931 chromaticity coordinates of the reflection spectra from S1 to S5 for c)  $x$ -polarization and d)  $y$ -polarization, respectively. The arrow indicates variation from S1 to S5.

hue- and saturation-tuned colors can also be achieved by varying  $P_x$  and  $P_y$  for  $y$ -polarized incidence, as shown in Figure 1d. Hence, the full color gamut can be covered with the use of two orthogonally polarized incident lights. Particularly, high-quality blue color can be obtained based on the designed architecture, which is not possible to realize with plasmonic or amorphous-silicon-based dielectric metasurfaces.<sup>[1–4,14,25]</sup>

To analyze the reflected characteristics of the nanopixels in different polarization states, we simulated the reflection spectra of five nanopixels (corresponding to the geometry parameters in the dashed box of Figure 1) for  $x$ - and  $y$ -polarization states in Figure 2a,b, respectively. The reflected spectra have a redshift with the increasing  $P_x$  for  $x$ -polarization. The central wavelengths of the reflected spectra are 485, 515, 550, 580, and 610 nm, respectively, when the nanostructure varies from S1 to S5. The efficiency can also remain as high as  $\approx 100\%$  for the five nanostructures. However, the central wavelengths of the reflected spectra will not have an apparent shift for the same five nanostructures for  $y$ -polarization. Certainly, the efficiency and bandwidth of the reflected spectra have a slight difference. According to the color-mixing principle, saturation indicates the proportion of monochromatic light (solid color) with respect to white light, namely, of the purity of colors.<sup>[33]</sup> In this content, the narrower bandwidth of spectra will lead to higher saturation with an increase in the ratio of monochromatic

light. Figure 2c,d shows the CIE 1931 chromaticity coordinates, which include the five colors generated from S1 to S5 for  $x$ - and  $y$ -polarization states, respectively. The approach of calculating CIE XYZ tristimulus from reflection spectra is given in Supporting Information. The chromaticity diagram of  $x$ -polarization in Figure 2c has significantly different hues ranging from blue ( $206^\circ$ ) to red ( $357^\circ$ ) due to the presence of various central wavelengths across the entire visible region. In contrast, the saturation of the colors in Figure 2d exhibits significantly decreasing trend from S1 (75.8%) to S5 (48.5%), where the central wavelength shifts only about 10 nm. Thus, we simultaneously realize the hue- and saturation-tuned structural colors under two orthogonally polarization states, which is desirable for practical applications such as 3D displaying and data storage.

To investigate the relation between the incident angle and the resonant peak, we calculated the contour map of the reflected efficiency as a function of the wavelength and the incident angle under two polarization states for the periodic structure with  $P_x = 350$  nm and  $P_y = 300$  nm in Figure 3a,b, respectively. For nearly all incident angles from  $0^\circ$  to  $80^\circ$ , the central resonant peaks are 550 and 490 nm for  $x$ - and  $y$ -polarizations, respectively. However, the efficiency of the central resonant peak gradually decreases as the incident angle increases, with the efficiency being approximately 80% for  $32^\circ$  and

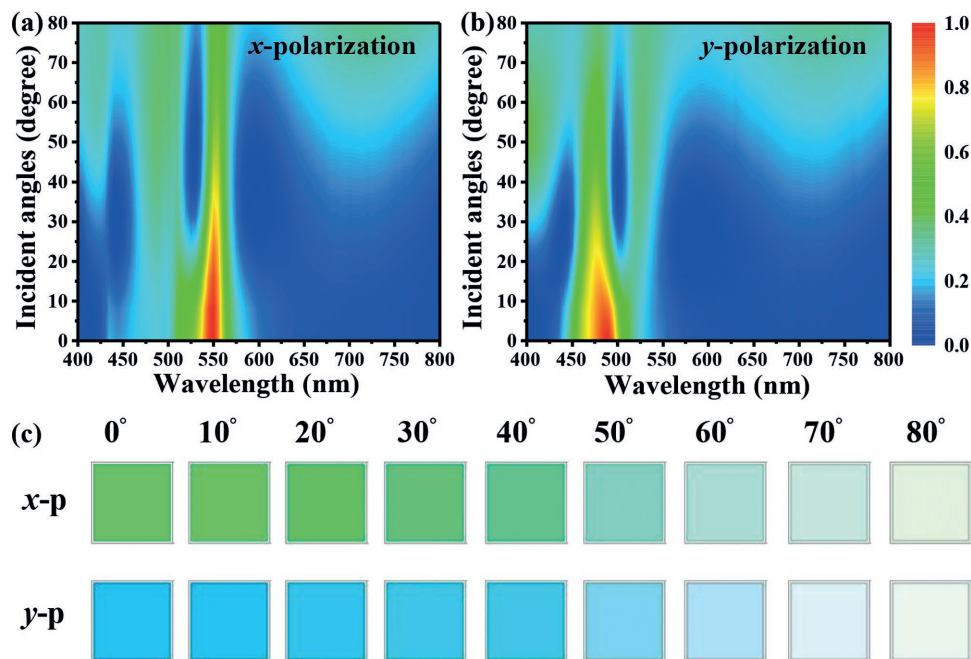


**Figure 3.** The sensitivity of incident light. Simulated reflection spectra maps of S3 ( $P_x = 350$  nm) as a function of wavelength and incident angle for a) x-polarization and b) y-polarization. c) Corresponding colors of the structure for varying incident angles in a step of 10°.

40% for 80°. Meanwhile, when the incident angle exceeds 40°, a certain small resonance around the central resonant peak will occur and gradually expand in the spectrum. The monochromaticity of reflected light gradually decreases, resulting in the reduced saturation. The corresponding colors under oblique incident light with a 10° interval are shown in Figure 3c. The colors under x- and y-polarization states basically remain unchanged from 0° to 40°. The saturation of colors under both polarization states gradually reach 0% (white light) when the oblique incident angle is 80°. Hence, the angular tolerance of the nanostructure is at least 40°. The proposed nanostructures can be applied as small-angle displays. Moreover, when the incident angle is greater than 40°, the saturation of colors varies apparently from 66.20 to 0.04% by tuning incident angle, which can be used as a wide-angle detector and an angle-sensitive microscope.

To further explore the mechanism of light-matter interaction of the reflection spectra, we simulated the magnetic field distribution at resonant wavelengths of 490 and 550 nm under two polarization states for S3 in Figure 4. Figure 4a,b shows the magnetic field distributions  $|H|$  in the  $x$ - $z$  plane at wavelengths of 490 and 550 nm for x-polarized incident light, respectively. Figure 4c,d shows the magnetic field distributions  $|H|$  in the  $x$ - $z$  plane at wavelengths of 490 and 550 nm for y-polarized incident light, respectively. Obviously, the magnetic field profiles of the two polarization states at resonant wavelength (Figure 4b,c) are the strongest at the center of nanopixel and the weakest in the vicinity of the nanopixel. This indicates that the magnetic field is strongly confined in the  $\text{TiO}_2$  pillars. The magnetic field is weak and primarily located in the interior of  $\text{TiO}_2$  pillar for the nonresonant wavelength (Figure 4a,d). The resonant mechanisms for both polarization states are identical. It primarily

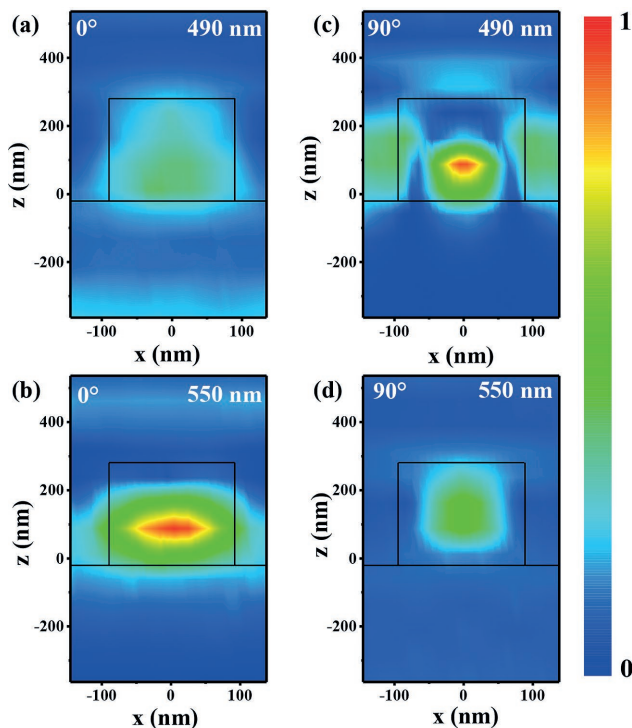


**Figure 4.** Simulated magnetic field distributions  $|H|$  at resonant wavelengths (490 and 550 nm) of S3 under the two polarization states. Non-resonant magnetic field distributions in the  $x$ - $z$  plane a) at wavelength 490 nm under x-polarization and d) at wavelength 550 nm under y-polarization. Resonant magnetic field distributions in the  $x$ - $z$  plane b) at wavelength 550 nm under x-polarization and c) at wavelength 490 nm under y-polarization, respectively.

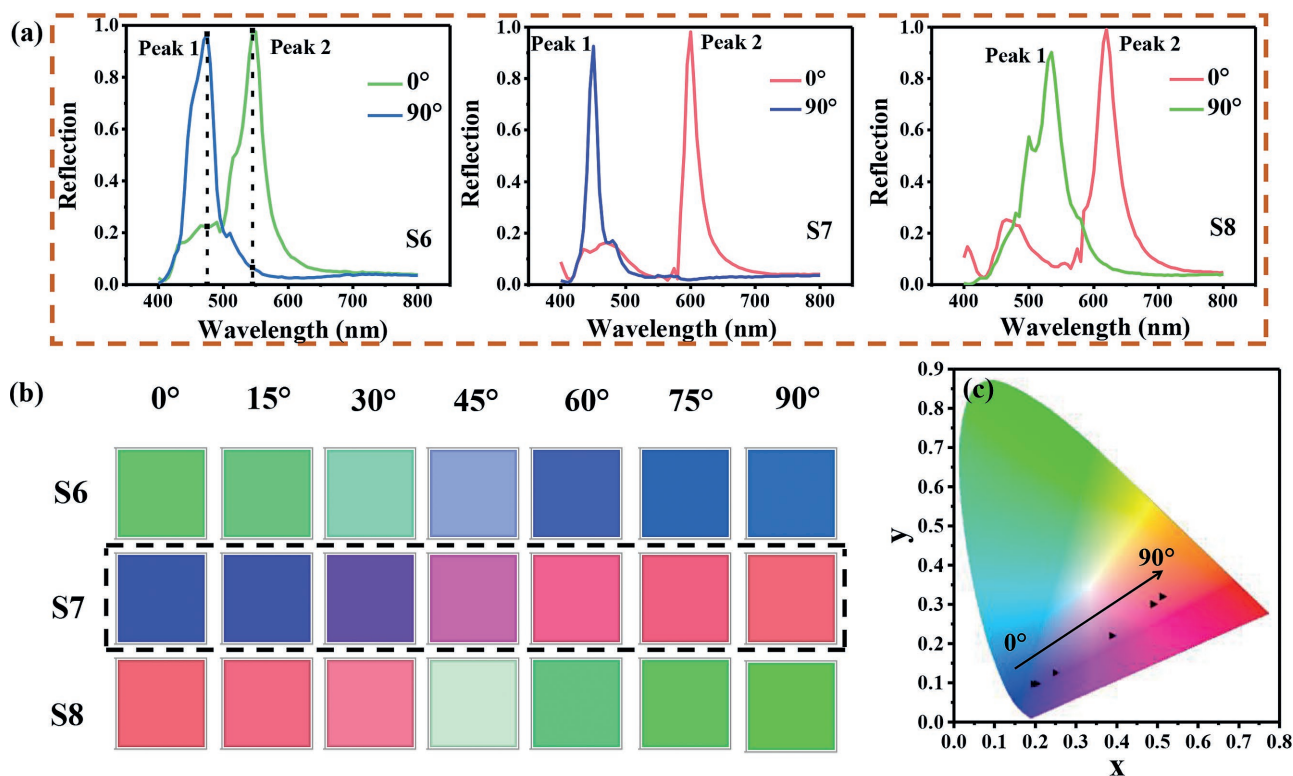


**Figure 5.** RGB switching of designed pixel arrays as a function of the incident polarization angle. a) Simulated reflection spectra of green-blue (G-B) structure, blue-red (B-R) structure, and red-green (R-G) structure in that order. For each structure, the color changes significantly under x-polarization and y-polarization. b) Corresponding reflection-mode color responses of three designed structures for varying incident polarization angles in a step of 15°. c) Corresponding CIE 1931 chromaticity coordinates for spectra of pixels indicated by the dashed box in (b) (B-R structure). The arrow indicates variation in the polarization angle from 0° to 90°.

relies on the intrinsic properties of titanium oxide, which can support dipole resonances and form photonic band gaps due to the significant refractive index difference between TiO<sub>2</sub> and silica via periodic array.<sup>[29]</sup> In addition, the white light incidence on the periodic structure excites a guided mode via light-matter interaction on the surface. The mode leaks into the surrounding environment and interacts with directly reflected light. The interference between directly reflected light and radiated light results in Fano resonance with high quality and a sharp peak.<sup>[10]</sup> The effects of Fano resonance along with the presence of the photonic band gap lead to improved reflection spectra, which can be utilized to generate preferable color impressions.

Since an apparent color contrast of x- and y-polarization states can be obtained with varying periods, we can also realize three-primary-color switching for two orthogonally polarized incident lights, which is significant for data storage and display technologies. **Figure 5** gives three nanostructures corresponding to S6 (green-blue [G-B] structure with  $P_x = 350$  nm,  $P_y = 300$  nm,  $a = 220$  nm,  $b = 160$  nm), S7 (blue-red [B-R] structure with  $P_x = 300$  nm,  $P_y = 400$  nm,  $a = 140$  nm,  $b = 260$  nm), and S8 (red-green [R-G] structure with  $P_x = 400$  nm,  $P_y = 340$  nm,  $a = 260$  nm,  $b = 180$  nm), respectively. **Figure 5a** shows the reflection spectra of three nanostructures, whose peak 1 and peak 2 are located at 475 and 545 nm, 450 and 600 nm, and 535 and 620 nm for x- and y-polarized incident lights, respectively. Since the bandwidth of the reflection peak is narrow and the efficiency is more

than 90% for all three nanostructures, the six corresponding colors exhibit high purity and saturation. **Figure 5b** depicts the virtual colors generated by the three nanostructures for various polarization angles ranging from 0° to 90°. Obviously, the three nanostructures can achieve switching from green to blue, red to blue, and red to green via changes only in the polarization angles. The corresponding CIE 1931 chromaticity coordinates for the spectra of the B-R structure are shown in **Figure 5c**. The colors will gradually shift from blue to purple to red with varying polarization angles, which results from the reflected response to polarized light. According to Malus' law, we have

$$R(\varphi, \lambda) = R_v(\lambda) \sin^2 \varphi + R_h(\lambda) \cos^2 \varphi \quad (1)$$

where  $\varphi$  denotes the polarization angle of incident light and  $R_v/R_h$  is the reflectance for the electric field being vertical/parallel to the x-axis. When  $\varphi$  varies from 0° to 90°, the resonant peaks of reflection spectra shift at least 100 nm for the three nanostructures, which means that we can dynamically tune structural colors via varying the polarization angle of the incident light to obtain dual or multiple colors. The flexible switching of colors enables a signal nanopixel to encode dual- or multiple-information states in display technologies. In this context, our proposed nanostructures can be used to create micro image display containing high-density storage, digital displaying, and 3D displaying.

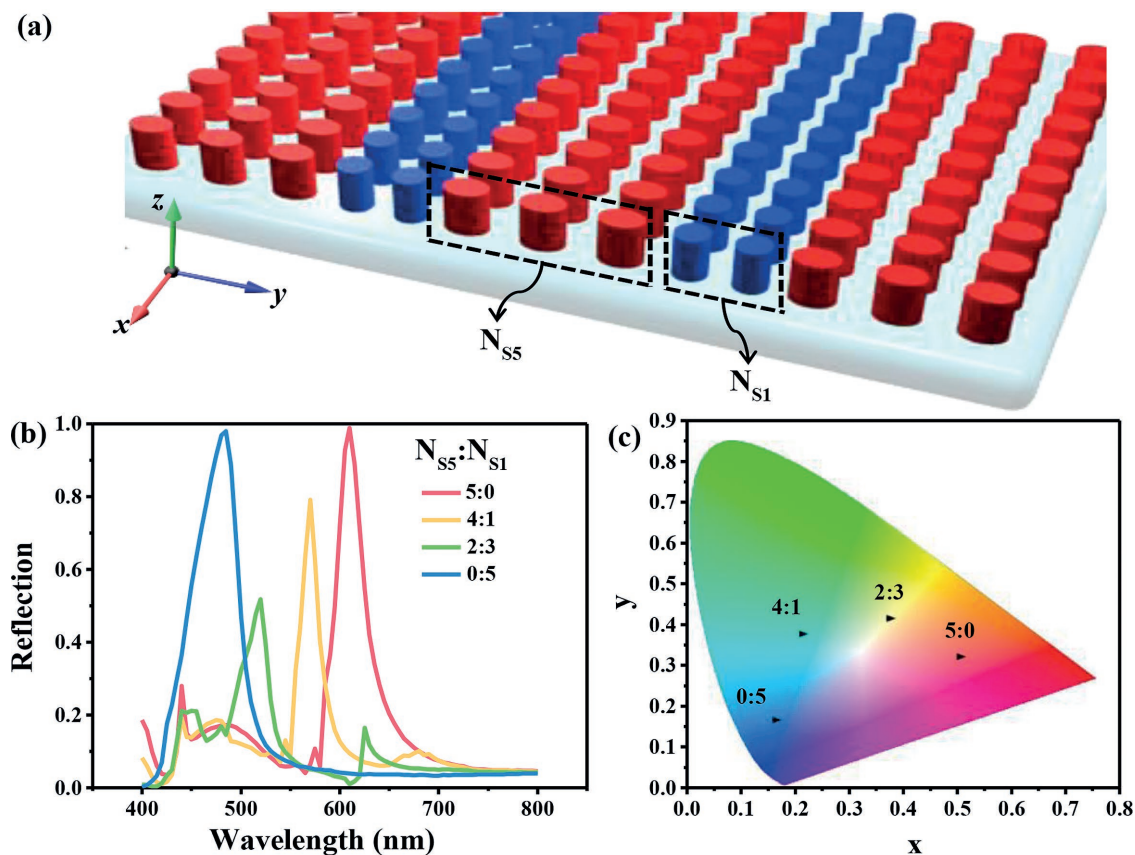


**Figure 6.** Mixing colors for varying ratios of two pixel types. a) The number of pixels for S1 and S5 are  $N_{S1}$  and  $N_{S5}$ , respectively. The colors can be tuned by different ratios of  $N_{S1}$  and  $N_{S5}$ . b) Simulated reflection spectra of the four mixed structures ( $N_{S5}:N_{S1}$ ). In all cases, the incident light is  $x$ -polarized. c) CIE 1931 chromaticity coordinates for spectra of mixed structures.

Aside from the realization of RGB switching via meticulous design, we next consider probing the mixing principle of colors. As an example, two types of nanostructures (S5 and S1 in Figure 1) are arrayed with distinct mixing ratios  $N_{S5}:N_{S1}$  (5:0, 4:1, 2:3, and 0:5 in that order) under  $x$ -polarized incident light, as illustrated in Figure 6a. As mentioned previously, the individual S1 structure is the blue color pixels while the S5 structure is red color pixels. Figure 6b illustrates the simulated reflected spectra for the four mixing ratios. The resonant peak of the spectrum is gradually observed to redshift over the range from 485 nm (0:5), 520 nm (2:3), and 570 nm (4:1) to 610 nm (5:0), covering three primary colors of blue, green, and red. The efficiencies of the mixed colors are 99%, 79%, 51%, and 98% in that order. The corresponding CIE 1931 chromaticity coordinates for the four ratios are shown in Figure 6c. Given the coupling effects between the five pixels, the mixed reflected spectra for ratios 4:1 and 2:3 do not perfectly correspond to the linear combination of S1 and S5. Several distinct colors can be obtained by adjusting only the type, ratio, and dimensions of the pixels, which makes our approach potentially useful in digital displaying and imaging technologies.

In order to vividly highlight the range of color gamut that can be covered, and the hue-and-saturation tuning that can be realized, we use MATLAB to print an oil painting “Mother and Son” utilizing 137 kinds of colors generated by the nanostructures of

$\text{TiO}_2$ . They are composed of nanostructures by varying periods and diameters along two orthogonal directions. Figure 7a,b presents the structural colors of the reproduction under  $x$ - and  $y$ -polarization states, respectively. The colors in two polarization states are abundant, which can basically cover three primary colors. A striking contrast of colors can be seen under two polarization states, such as blue to green (the sky) and yellow to blue (the coat of the kid and the lining of the hats). Besides, the colors of both the woman’s scarf and the kid’s scarf are orange with different saturation (85.36% for kid’s scarf and 52.50% for woman’s scarf) under  $x$ -polarization. While when the incident light is the  $y$ -polarization state, the hue is  $9^\circ$  for kid’s scarf and  $174^\circ$  for woman’s scarf. Therefore, the hue-and-saturation tuning can be simultaneously realized in our study. As the hue and saturation can be manipulated under different polarizations, this technique may be developed into 3D imaging and displaying. Such polarization-dependent multicolor nanostructures could lead to ultrahigh-resolution 3D photographs, paintings, holograms, and anticounterfeiting measures.

In summary, we have demonstrated a polarization-sensitive color filter based on elliptical titanium oxide nanopixels on a silica substrate. Fano resonance can be obtained in this architecture via interference between the radiation waves of Mie dipole resonance and directly reflected waves, which leads to generation of narrowband-reflected spectra across the visible

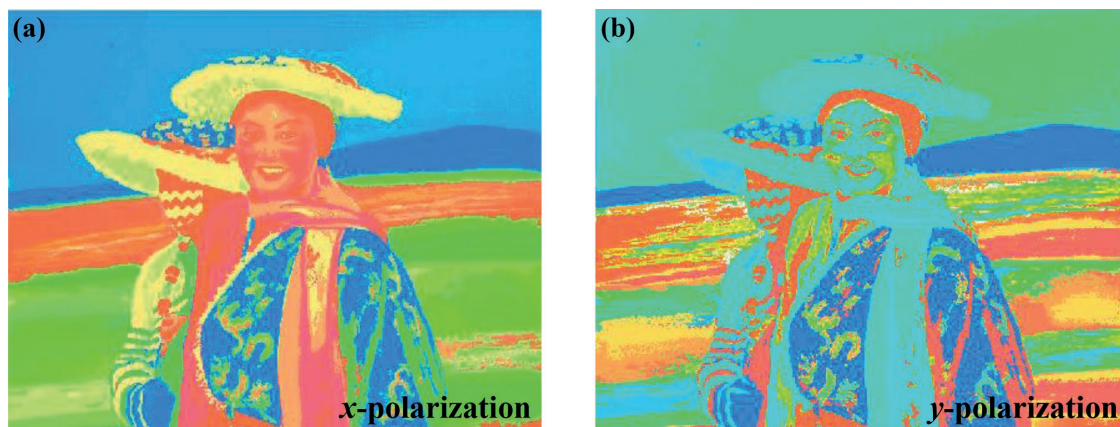


**Figure 7.** A reproduction of the painting “Mother and Son,” printed by Dong Wang. The colors in the reproduction are generated by the TiO<sub>2</sub> nanostructures with varying periods and diameters under a) *x*-polarized and b) *y*-polarized incident lights, respectively. The copyright permission has been obtained from the copyright holder.

spectrum. By tuning of the various nanopixel parameters, the high-saturation and high-resolution structural colors can be generated with oblique-incident-angle tolerance of up to  $\approx 40^\circ$  for both polarization states.

Particularly, compared with the previous research on structural colors utilizing TiO<sub>2</sub>,<sup>[29]</sup> we proposed a novel design strategy that can simultaneously tune hue and saturation. In the proposed nanostructures, we not only can vary the major and minor diameters of the ellipse but can also alter the periods in the *x*- and *y*-directions. The independent variation of periods along two directions ensures high efficiency (more than 90% theoretically) for varying polarization angles and considerable shift (150 nm or so) of the center wavelength under two orthogonally polarization states. By varying period and diameter only along one direction, we can obtain the hue tuning (from blue to red) under one polarization state and the saturation tuning (from 48.5 to 75.8% with basically constant hue) under vertical polarization state. The two attributes of hue and saturation, which are crucial for the perception of color by the human eyes, can be flexibly controlled under *x*- and *y*-polarization states based on the designed strategy. Besides, we can implement RGB switching with high-quality and high-efficiency colors by accurately designing the parameters of periods and diameters. Dual and multiple colors can be obtained via varying polarization angles under one nanostructure. Our results indicate the potential of our approach in many significant applications, such as information coding, cryptography, high-density optical data storage, polarimetry microscopy, security encryption, 3D displaying, and hyperspectral microscopy.

## Supporting Information

Supporting Information is available from the Wiley Online Library or from the author.

## Acknowledgements

This work was supported by the National Key Research and Development Program of China (Grant Nos. 2017YFA0303800 and 2016YFA0301102),

the Natural Science Foundation of China (Grant Nos. 11774186, 11574163, and 61378006), and the Natural Science Foundation of Tianjin (16JCQNJC01700).

## Conflict of Interest

The authors declare no conflict of interest.

## Keywords

dielectric metasurface, polarization, structural colors

Received: September 23, 2017

Revised: December 5, 2017

Published online:

- [1] Z. Li, A. W. Clark, J. M. Cooper, *ACS Nano* **2016**, *10*, 492.
- [2] S. J. Tan, L. Zhang, D. Zhu, X. M. Goh, Y. M. Wang, K. Kumar, C.-W. Qiu, J. K. W. Yang, *Nano Lett.* **2014**, *14*, 4023.
- [3] V. R. Shrestha, S. S. Lee, E. S. Kim, D.-Y. Choi, *Nano Lett.* **2014**, *14*, 6672.
- [4] J. S. Clausen, E. Højlund-Nielsen, A. B. Christiansen, S. Yazdi, M. Grajower, H. Taha, U. Levy, A. Kristensen, N. A. Mortensen, *Nano Lett.* **2014**, *14*, 4499.
- [5] Y.-K. R. Wu, A. E. Hollowell, C. Zhang, L. J. Guo, *Sci. Rep.* **2013**, *3*, 1194.
- [6] B. Zeng, Y. Gao, F. J. Bartoli, *Sci. Rep.* **2013**, *3*, 2840.
- [7] M. Miyata, H. Hatada, J. Takahara, *Nano Lett.* **2016**, *16*, 3166.
- [8] X. M. Goh, R. J. H. Ng, S. Wang, S. J. Tan, J. K. W. Yang, *ACS Photonics* **2016**, *3*, 1000.
- [9] X. M. Goh, Y. Zheng, S. J. Tan, L. Zhang, K. Kumar, C.-W. Qiu, J. K. W. Yang, *Nat. Commun.* **2014**, *5*, 5361.
- [10] Y. Shen, V. Rinnerbauer, I. Wang, V. Stelmakh, J. D. Joannopoulos, M. Soljacic, *ACS Photonics* **2015**, *2*, 27.
- [11] A. Kristensen, J. W. K. Yang, S. I. Bozhevolnyi, P. Nordlander, N. J. Halas, N. A. Mortensen, *Nat. Rev. Mater.* **2016**, *2*, 16088.
- [12] M. K. Hedayati, M. Elbahri, *Plasmonics* **2017**, *12*, 1463.
- [13] Y. Gu, L. Zhang, J. K. W. Yang, S. P. Yeo, C.-W. Qiu, *Nanoscale* **2015**, *7*, 6409.
- [14] A. S. Roberts, A. Pors, O. Albrektsen, S. I. Bozhevolnyi, *Nano Lett.* **2014**, *14*, 783.

- [15] Z. Li, S. Butun, K. Aydin, *ACS Photonics* **2015**, 2, 183.
- [16] V. R. Shrestha, S. S. Lee, E. S. Kim, D.-Y. Choi, *Sci. Rep.* **2015**, 5, 12450.
- [17] F. Cheng, J. Gao, L. Stan, D. Rosenmann, D. Czaplewski, X. Yang, *Opt. Express* **2015**, 23, 14552.
- [18] Z. Li, W. Wang, D. Rosenmann, D. A. Czaplewski, X. Yang, J. Gao, *Opt. Express* **2016**, 24, 20472.
- [19] A. Arbabi, Y. Horie, M. Bagheri, A. Faraon, *Nat. Nanotechnol.* **2015**, 10, 937.
- [20] M. Decker, I. Staude, M. Falkner, J. Dominguez, D. N. Neshev, I. Brener, T. Pertsch, Y. S. Kivshar, *Adv. Opt. Mater.* **2015**, 3, 813.
- [21] S. Jahani, Z. Jacob, *Nat. Nanotechnol.* **2016**, 11, 23.
- [22] D. Lin, P. Fan, E. Hasman, M. L. Brongersma, *Science* **2014**, 345, 298.
- [23] F. Aieta, M. A. Kats, P. Genevet, F. Capasso, *Science* **2015**, 347, 1342.
- [24] D. Sell, J. Yang, S. Doshay, K. Zhang, J. A. Fan, *ACS Photonics* **2016**, 3, 1919.
- [25] E. D. Palik (Ed.), *Handbook of Optical Constant of Solids*, Academic Press, San Diego, CA **1985**.
- [26] V. Flauraud, M. Reyes, R. Paniagua-Dominguez, A. I. Kuznetsov, J. Brugger, *ACS Photonics* **2017**, 4, 1913.
- [27] V. Vashistha, G. Vaidya, R. S. Hegde, A. E. Serebryannikov, N. Bonod, M. Krawczyk, *ACS Photonics* **2017**, 4, 1076.
- [28] P. Gutruf, C. Zou, W. Withayachumnankul, M. Bhaskaran, S. Sriram, C. Fumeaux, *ACS Nano* **2015**, 10, 133.
- [29] S. Sun, Z. Zhou, C. Zhang, Y. Gao, Z. Duan, S. Xiao, Q. Song, *ACS Nano* **2017**, 11, 4445.
- [30] M. Khorasaninejad, A. Y. Zhu, C. Roques-Carmes, W. T. Chen, J. Oh, I. Mishra, R. C. Devlin, F. Capasso, *Nano Lett.* **2016**, 16, 7229.
- [31] R. C. Devlin, M. Khorasaninejad, W. T. Chen, J. Oh, F. Capasso, *Proc. Natl. Acad. Sci. USA* **2016**, 113, 10473.
- [32] COMSOL Multiphysics, Version 5.0, COMSOL, Inc., Burlington, MA **2016**.
- [33] V. R. Shrestha, C. S. Park, S.-S. Lee, *Opt. Express* **2014**, 22, 3691.